Solar spectral actinic flux and photolysis frequency measurements in a deciduous forest

B. Bohn[1]

Received 21 November 2005; revised 28 March 2006; accepted 4 May 2006; published 8 August 2006.

[1] Within the Emission and Chemical Transformation of Biogenic Volatile Organic Compounds (ECHO) project the photochemistry of biogenic organic compounds in a forest was investigated. In this context, two spectroradiometers were used to determine solar spectral actinic flux and photolysis frequencies within and above a deciduous forest at Jülich, Germany. Locations in the forest and in a small clearing were examined 2 m above ground. Under overcast conditions, photolysis frequencies were within 1–3% and 6–8% of above canopy values at forest and clearing locations, respectively. In a spectral range below 500 nm the canopy was found to act as a gray filter that diminished spectral actinic flux independent of daytime and wavelength. Under clear-sky conditions, diurnal variations within the forest also followed that of diffuse sky radiation above the forest except for sharp peaks from direct sunlight that was incident sporadically at the selected locations. The results under all conditions were in accord with the foliage being opaque toward UV and gaps in the canopy being responsible for the remaining actinic flux. Sky photographs showed that the distribution and size of gaps in the foliage were extremely heterogeneous with patterns changing rapidly upon changing location. Regarding daytime chemical reactions of biogenic compounds within the forest, it was estimated that degradation by OH was reduced by a factor similar to the photolysis frequencies, while potential degradation by NO_3 was increased by a factor of $\sim$3 compared with above forest conditions. As a result, it was estimated that minor fractions of 0.8% of isoprene and 3.4% of monoterpenes were degraded by reactions with OH, NO_3, and O_3 prior to transport into the layer above the forest.

Citation: Bohn, B. (2006), Solar spectral actinic flux and photolysis frequency measurements in a deciduous forest, *J. Geophys. Res.*, *111*, D15303, doi:10.1029/2005JD006902.

1. Introduction

[2] Forests represent a major source of biogenic organic volatile compounds (BVOCs) in the troposphere, most importantly isoprene, terpenes, sesquiterpenes, and oxygenated compounds like alcohols and aldehydes [e.g., *Guenther et al.*, 1995]. Emissions and deposition of trace gases by forests are controlled by many time-dependent parameters including meteorological conditions (e.g., light and temperature), soil properties (e.g., water availability) and the composition of the plant inventories (e.g., broadleaf trees or conifers) [*Guenther et al.*, 2000; *Fuentes et al.*, 2000]. Owing to this complexity, the impact of BVOC emissions from forests on atmospheric photochemistry, including aerosol formation, are currently not well understood and consequently the regional and global effects on air quality and climate are uncertain.

[3] The Emission and Chemical Transformation of Biogenic Volatile Organic Compounds (ECHO) project aimed to investigate the influence of BVOC emissions on tropospheric photochemistry by combined measurement and modeling activities studying emissions, transport and transformation of trace gases in a typical European mixed forest at Jülich, Germany (50.91°N, 6.41°E). In two field campaigns during the summer seasons of 2002 and 2003 a wide range of instrumentation was used at a tower set up in the forest [*Ammann et al.*, 2004; *Kleffmann et al.*, 2005; *Spirig et al.*, 2005]. Measurements covered of a broad spectrum of organic compounds (including organic nitrates), HO_x (OH, HO_2), RO_2 and NO_3 radicals, O_3, NO_x (NO, NO_2), aerosols, meteorological parameters and photolysis frequencies. These activities were complemented by modeling studies and simulation experiments utilizing the atmosphere simulation chamber SAPHIR at Forschungszentrum Jülich, and a wind tunnel at Hamburg University [*Aubrun and Leitl*, 2004; *Aubrun et al.*, 2005].

[4] Photolysis processes are a key aspect of tropospheric chemistry because photolyses by solar UV produce reactive radicals, most importantly the OH radical. OH radicals largely initiate the degradation of many trace gases including BVOCs. The degradations proceed in terms of complex chain reactions where OH is regenerated from secondarily formed HO_2 in reactions with NO or O_3. The primary

[1]Institut für Chemie und Dynamik der Geosphäre II: Troposphäre, Forschungszentrum Jülich, Jülich, Germany.

0148-0227/06/2005JD006902

Table 1. Selection of Important Tropospheric Photolysis Processes, Wavelength Ranges, and Local Noon Clear-Sky Photolysis Frequencies (Above the Forest) on 19 July 2003 at Jülich, Germany[a]

Notation	Process	Range, nm	j, s^{-1}	Error, %
$j(O^1D)$	$O_3 \rightarrow O(^1D) + O_2$	295–325	2.4×10^{-5}	15
$j(H_2O_2)$	$H_2O_2 \rightarrow OH + OH$	300–380	8.3×10^{-6}	10
$j(HCHO)_r$	$HCHO \rightarrow H + HCO$	300–335	2.8×10^{-5}	20
$j(HCHO)_m$	$HCHO \rightarrow H_2 + CO$	310–360	3.4×10^{-5}	20
j(HONO)	$HONO \rightarrow OH + NO$	320–400	1.4×10^{-3}	20
$j(NO_2)$	$NO_2 \rightarrow O(^3P) + NO$	310–420	7.9×10^{-3}	10
$j(NO_3)_r$	$NO_3 \rightarrow O(^3P) + NO_2$	400–620	1.7×10^{-1}	15
$j(NO_3)_m$	$NO_3 \rightarrow NO + O_2$	580–620	2.1×10^{-2}	15

[a]Lower indices r (radical) and m (molecular) denote formation of different photoproducts from the same precursor. Wavelength ranges are approximate (tropospheric conditions). Molecular data σ and ϕ (equation (5)) were taken from literature. O_3, *Malicet et al.* [1995] and *Matsumi et al.* [2002]; H_2O_2, *Sander et al.* [2003], $\phi(OH) = 2.0$; HCHO, *Meller and Moortgat* [2000] and *Atkinson et al.* [2004]; HONO, *Bongartz et al.* [1994], $\phi = 1.0$; NO_2, *Merienne et al.* [1995] and *Troe* [2000]; and NO_3, *Atkinson et al.* [2004]. Error estimates include a 6% contribution from the actinic flux measurements and estimated 298 K uncertainties of σ and ϕ from literature.

radical productions in photolysis processes are essential to initiate the chain reactions and to compensate for radical losses by terminating reactions, e.g., by OH + NO_2 and HO_2 + HO_2. For example, a large fraction of primary production of OH results from reaction of electronically excited $O(^1D)$ with water vapor,

$$O(^1D) + H_2O \longrightarrow 2OH \quad (1)$$

where $O(^1D)$ is produced in the UV photolysis of ozone:

$$O_3 + h\nu(\lambda \leq 340\ \text{nm}) \longrightarrow O(^1D) + O_2 \quad (2)$$

Moreover, tropospheric ozone is formed to a large extent by the photolysis of NO_2 followed by the reaction of ground state $O(^3P)$ with O_2:

$$NO_2 + h\nu(\lambda \leq 430\ \text{nm}) \rightarrow NO + O(^3P) \quad (3)$$

$$O(^3P) + O_2 + M \rightarrow O_3 + M \quad (4)$$

Thus a quantitative treatment of photolysis processes is required for an understanding of tropospheric photochemistry. Reaction (3) for example is quantified by a first-order rate constant $j(NO_2)$ referred to as photolysis frequency:

$$j(NO_2) = -\frac{d[NO_2]}{dt}\frac{1}{[NO_2]} = \int \sigma(NO_2)\phi(NO)F_\lambda d\lambda \quad (5)$$

[5] The first part of the equation gives a chemical definition of the photolysis frequency in the absence of other NO_2 loss or production processes. This definition is therefore not suitable for a determination of $j(NO_2)$ by measurements of NO_2 in complex chemical systems like the troposphere. However, it can be used in simpler, artificial systems like chemical actinometers [e.g., *Shetter et al.*, 2003]. The second part of equation (5) shows the relation with the radiometric quantity spectral actinic photon flux (F_λ) and the molecular properties of NO_2, namely, absorption cross section $\sigma(NO_2)$ and quantum yield $\phi(NO)$ of NO + $O(^3P)$ formation that are a function of wavelength (λ). Photolysis frequencies of other photolysis processes are defined accordingly. In Table 1 a selection of important photolysis processes is listed as well as local noon values of photolysis frequencies above the forest on a clear-sky day of the 2003 ECHO campaign. Besides ozone, nitrous acid (HONO) and formaldehyde (HCHO) are important photolytic precursors of tropospheric HO_x.

[6] Spectral actinic flux F_λ is strongly variable under natural conditions depending on wavelength, solar zenith angle and atmospheric variables like cloud cover, aerosol load and ozone column. Ground based spectral actinic flux measurements aiming at photolysis frequencies are usually made at sites providing full view of the upper hemisphere. To the knowledge of the author so far no measurements have been reported from within forests. Previous work considering radiometric quantities within forests concentrated on photosynthetic active radiation (PAR, 400–700 nm) influencing the biological activity of plants [e.g., *Myneni*, 1991] and on measurements of the leaf area index (LAI) rather than photochemistry [e.g., *Chen and Cihlar*, 1995; *Chen et al.*, 1997]. Moreover, the radiometric quantity usually considered in the PAR and UV range is irradiance (E_λ) rather than actinic flux [e.g., *Heisler et al.*, 2003]. The fundamental difference between these quantities is that irradiance is describing photon (or energy) flux with respect to flat surfaces (e.g., leaves) by weighting spectral radiance L_λ with the cosine of the polar angle ϑ upon integration over the solid angle field of view (φ = azimuth angle):

$$E_\lambda = \int_0^{2\pi}\int_0^{\pi} L_\lambda(\lambda,\vartheta,\varphi)\cos(\vartheta)\sin(\vartheta)d\vartheta d\varphi \quad (6)$$

In contrast there is no such weighting in the calculation of spectral actinic flux in accordance with the reception characteristics of molecules:

$$F_\lambda = \int_0^{2\pi}\int_0^{\pi} L_\lambda(\lambda,\vartheta,\varphi)\sin(\vartheta)d\vartheta d\varphi \quad (7)$$

The relationship between spectral actinic flux and irradiance is complex under natural conditions in particular when parts of the sky are blocked by opaque objects, e.g., trees.

[7] The question addressed in this work is to what extend UV spectral actinic flux was reduced within the forest at the ECHO field site and how this reduction affected photolysis frequencies. This was a prerequisite for modeling studies

Figure 1. Spectroradiometer detector heads and shadow ring. The picture was taken at the site of the measurements above the forest before the 2003 campaign. The two heads in front belonged to the instrument that was then moved into the nearby forest.

investigating local photochemistry based on combined observations of radical species, trace gases and meteorological parameters as intended within the ECHO project. The discussion is focused on the photolysis frequencies $j(O^1D)$ and $j(NO_2)$ which are governed by the wavelength ranges UV-B (300–320 nm) and UV-A (320–400 nm) in good approximation. The results of this work were complemented by profile measurements and long-term measurements of photolysis frequencies at different levels of the ECHO tower using filter radiometers [*Bohn et al.*, 2006].

2. Experimental Method

2.1. Spectroradiometer

[8] Two spectroradiometers similar in construction were used for parallel measurements of downwelling 2 π sr spectral actinic flux within and above the forest. The instruments were based on thermostated double monochromators (Bentham, DTM 300) [*Hofzumahaus et al.*, 1999]. For each instrument, two 10 m quartz fibers were guiding light from the entrance optics to the monochromators where fiber cross sections were converted from round to rectangular to feed the monochromator entrances without losses. Cochannel operation was achieved in both instruments by utilizing the total slit height of the monochromators (20 mm) for two separate optical paths with slit heights of 7 mm separated by an unused section of 6 mm. In this setup, cross talk between the channels was found to be 0.3% or less. Entrance optics were specially designed for actinic flux reception in one hemisphere with direction-independent sensitivity using quartz domes (see Figure 1). UV sensitive photomultiplier tubes (EMI, 9250 QB) were used for light detection. A spectral resolution and a step size of 1 nm were used in the most important wavelength range 280–420 nm. Absolute calibration of the spectroradiometers was achieved using a 1000 W irradiance standard (BN-9101, Gigahertz-Optik, PTB traceable) and 45 W secondary standards (Optronic Laboratories) for regular checks. The accuracy of the measured spectral actinic flux was 5–7% considering the uncertainty of the irradiance standard and the characterization of the inlet optics. More information on technical details of the spectroradiometers and uncertainties regarding different photolysis frequencies are given by *Hofzumahaus et al.* [1999, 2002]. Estimated total uncertainties are listed in Table 1. A constant temperature of 298 K was assumed in the calculation of photolysis frequencies from the actinic flux spectra (equation (5)) to keep the influences of ambient temperature and foliage separated.

[9] Measurements of upwelling radiation were not included in the present study for technical reasons and because the spectral albedo of vegetation-covered surfaces is generally low in the UV range (1–4%) [*Feister and Grewe*, 1995; *Webb et al.*, 2004]. However, for the visible range spectral actinic flux may have been enhanced by 5–10% above the forest caused by an increased albedo in this spectral range [*Feister and Grewe*, 1995].

2.1.1. Above Forest Measurements

[10] For reasons of convenience, measurements above the forest were made on top of a building 370 m away from the forest site in southerly direction. A shadow ring was used with one channel to distinguish between direct sunlight and diffuse sky radiation. The setup of the ring is shown in Figure 1. Actinic flux from diffuse sky radiation was measured by the shaded detector and corrected with respect to the solid angle blocked by the ring. Subtraction from the total actinic flux received by the other channel allows to calculate the contribution from direct sunlight. The shadow ring correction was based on the assumption of a time-independent, isotropic radiance distribution. This introduced errors regarding the relative contributions of direct and diffuse sunlight. However, dependent on external conditions, these errors were estimated to be 5% or less [*Bohn and Zilken*, 2005].

[11] A scanning range 280–550 nm was selected for the measurements above the forest. The upper limit was determined by the decreasing quantum yields of the UV sensitive photomultipliers. In order to save scanning time, 2 nm steps were used in the range 420–550 nm. The corresponding scanning times were about 3 min. The use of wavelength steps of about twice the full width at half maximum in the range 420–550 nm was accepted because this range was considered secondary for photolysis processes. Except for sporadic instrument failures and breaks for regular calibration, measurements were made continuously while solar zenith angles (χ) were smaller than 96°. Measurement periods are listed in Table 2.

[12] During four weeks of the 2003 campaign also a diode array spectroradiometer (Meteorologie Consult GmbH, Königstein, Germany) was used to measure spectral actinic flux above the forest. This instrument used a similar inlet optic but a combination of a single monochromator and a diode array to measure in a wavelength range 290–700 nm. The spectral resolution was about 2 nm at a pixel width of 0.8 nm. The main advantage of this instrument was the simultaneousness of the measurements in a wide range of wavelengths (also covering $j(NO_3)$) with high time resolution. In this study 1 min averages were recorded.

[13] Above forest measurements of photolysis frequencies were also made on top of the tower at the forest site using $j(NO_2)$ and $j(O^1D)$ filter radiometers [*Bohn et al.*, 2006]. These measurements were made with a high time resolution of 5–7 s. For comparison with the spectroradi-

Table 2. Notations of Spectroradiometer Measurement Positions Within and Above the Forest at Different Campaign Periods[a]

Period	Channel 1	Channel 2
	Spectroradiometer 1 (SR 1, Forest)	
15 Jun to 4 Jul 2002	forest 1 (25 NW)	clearing 1 (7 NW)
6–24 Jul 2002	forest 2 (15 SSE)	clearing 2 (5 S)
28 Jun to 9 Jul 2003	forest 3a (22 ESE)	forest 3b (19 ESE)
10 Jul to 19 Aug 2003	forest 4 (20 SE)	clearing 2 (5 S)
	Spectroradiometer 2 (SR 2, Roof)	
15 Jun to 29 Jul 2002	total (370 SSW)	diffuse[b] (370 SSW)
30 Jun to 19 Aug 2003	total (370 SSW)	diffuse[b] (370 SSW)
	Spectroradiometer 3 (Diode Array, SR 3, Roof)	
18 Jul to 18 Aug 2003	diode[c] (370 SSW)	–

[a]Distances, m, and directions relative to the ECHO tower at the clearing center are given in parentheses. See Figure 2 for comparison.
[b]Measurements with shadow ring.
[c]Total measurements up to 700 nm.

ometer, these data were averaged over the corresponding intervals during the spectroradiometer scans.

2.1.2. Forest Measurements

[14] For the forest measurements the scanning range was extended to 280–750 nm. This was accomplished by a further split of the light paths behind the exit slit to feed two additional, red-sensitive photomultipliers (EMI, 9659) protected by cutoff filters (~480 nm, Schott) to avoid second-order detection. Above 550 nm a different set of gratings was used reducing spectral resolution to about 2 nm. Caused by the extension of the wavelength range, scanning times were about 4.5 min. For comparison with the above canopy measurements the data were therefore synchronized by linear interpolations.

[15] In the forest the wavelength range was extended to cover the spectral region responsible for NO_3 photolysis (Table 1). In contrast to above canopy daytime conditions where $j(NO_3)$ was considered secondary because of low NO_3 concentrations (diminished by photolysis and reaction with NO) this could not be presumed for forest conditions. The spectral range 620–750 nm was included for the sake of completeness to cover PAR and visible radiation (400–750 nm) for potential applications not related to photochemistry.

2.2. Field Site and Sky Photography

[16] The instrument operated within the forest was installed in a water-tight housing for outdoor operation. It was located close to the edge of a clearing hosting the ECHO main tower. Figure 2 shows a map of the area and a close-up view of the tower surroundings. The clearing was situated next to a narrow road leading through the forest. The gap in the canopy was almost circular with a diameter of about 15 m. The forest surrounding the ECHO main tower was dominated by large beeches (*Fagus sylvatica*) of about 30 m height. Within a distance of about 50 m there were also some oaks (*Quercus robur*), birches (*Betula pendula*) and smaller spruce (*Picea abies*). Positions in the clearing and in forest unaffected by the clearing were accessible simultaneously within the 10 m quartz fiber ranges. Measurements were made 2 m above ground. During the campaigns positions were changed once to characterize different locations. The measurement sites were denoted forest 1–4 and

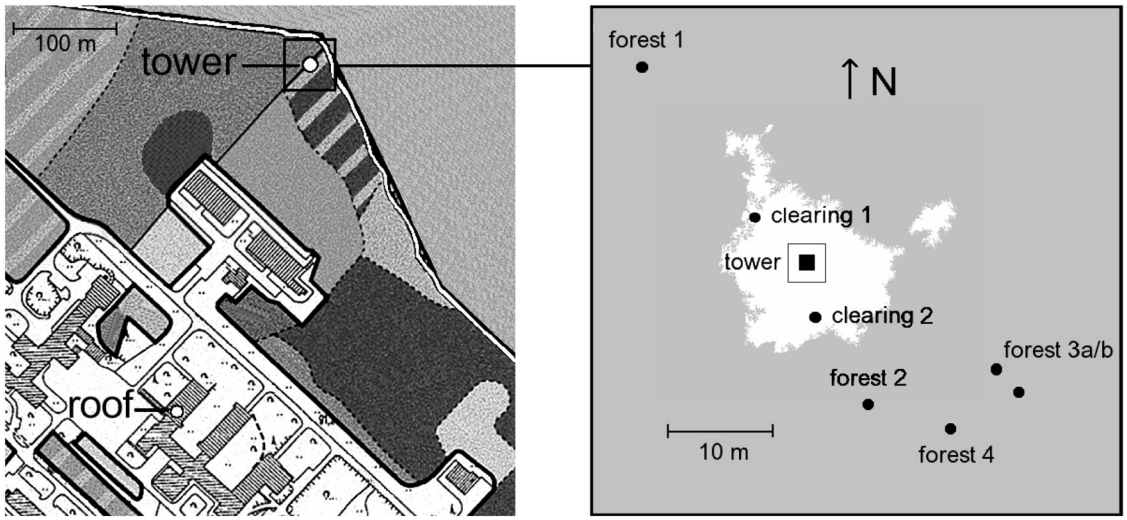

Figure 2. Map of measurement positions listed in Table 2. (left) Overview of the forest at Forschungszentrum Jülich. Hatched areas mark buildings, and gray areas represent forest stands of different compositions. Positions of the tower and the roof site were indicated. (right) Enlargement of the tower surroundings with measurement positions. The bright area marks the approximate extension of the clearing from a fish-eye photograph.

Figure 3. Fish-eye summer photograph of forest position 4 (2003).

Figure 4. Fish-eye winter photograph of forest position 4 (2003).

clearing 1–2. Table 2 and Figure 2 give an overview on relative positions and the respective time periods. Forest 3a and 3b denote two sites that were in direct vicinity to an instrument measuring OH and HO_2 radical concentrations within the forest. Except for this period radical measurements were made in the clearing at different levels of the tower [*Kleffmann et al.*, 2005].

[17] LAI measurements in the forest surrounding the main tower gave a mean value LAI = 5.7 [*Ammann et al.*, 2004]. The LAI corresponds to the one-sided area of leaves per unit ground area. The measured LAI was in reasonable agreement with averaged data for temperate deciduous broadleaf forests (5.1 ± 1.8) [*Scurlock et al.*, 2001]. Sky photographs were made to further characterize the measurement sites within the forest by reproducing the angular distributions of gap patterns in the canopy. A conventional camera (Nikon, FM) was used with a suitable objective (Nikkor, fisheye 16 mm f 2.8 D). This combination covered an about 180° field of view along the diagonal of the 24 × 36 mm film. The photographs were taken by directing the camera toward the zenith. The camera was then rotated by 90° to cover higher polar angles also in other directions. The resulting photographs were merged to create a single photograph with reasonable coverage of the upper hemisphere. Photographs were taken during winter and summer seasons to assess the effects of foliage. Examples are shown in Figures 3 and 4.

3. Results and Discussion

3.1. Above Forest Measurements

3.1.1. Contributions of Direct and Diffuse Sunlight

[18] Figure 5 shows two examples of actinic flux spectra obtained above the forest under clear-sky conditions. Total actinic flux as well as contributions of direct sunlight and diffuse sky radiation are shown. At local noon (~1140 UTC)

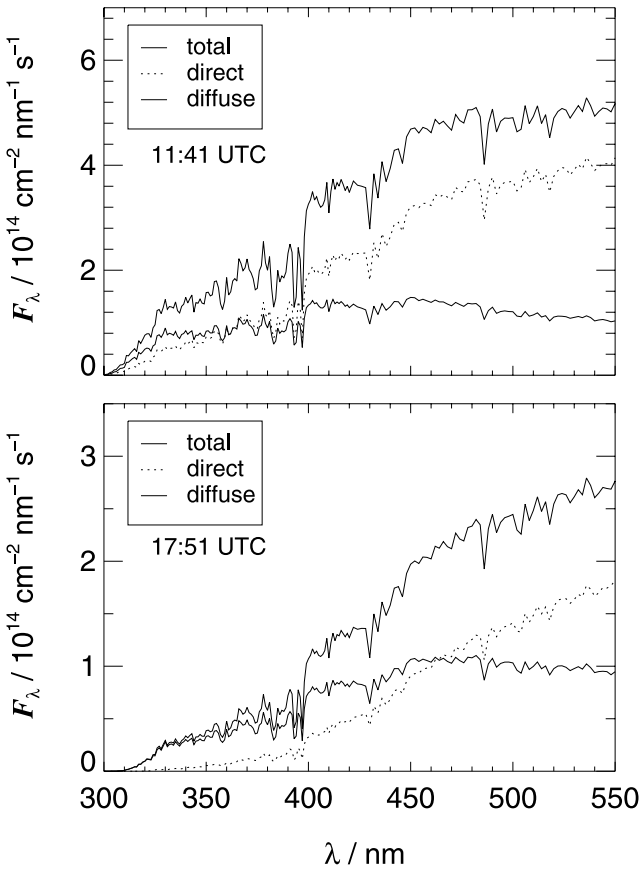

Figure 5. Actinic flux spectra at different times of day on 15 July 2003 (clear-sky conditions). Total actinic flux and contributions of diffuse sky radiation and direct sunlight are shown. (top) Local noon (χ = 29°), (bottom) late afternoon (χ = 75°).

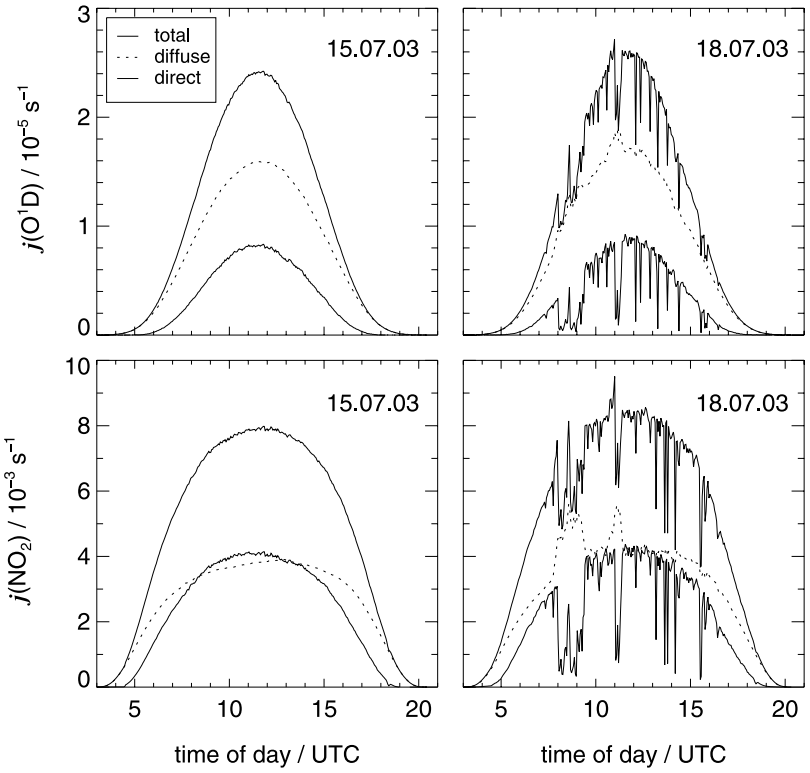

Figure 6. Diurnal variations of $j(O^1D)$ and $j(NO_2)$ on (left) 15 July 2003 (clear-sky conditions) and (right) 18 July 2003 (broken cloud conditions with low cloud cover).

a minimum solar zenith angle of 29° was reached on that day (15 July 2003). Accordingly, actinic flux and direct sunlight were at a maximum at this time of day. The contribution of direct sunlight is generally increasing with wavelength caused by decreasing losses by Rayleigh scattering. Moreover, the fluxes under clear-sky conditions are dependent on aerosol optical depths and ozone columns (UV-B). For comparison, Figure 5 (bottom) shows spectra on the same day in the late afternoon at a solar zenith angle of 75°. Fluxes were much lower compared with local noon conditions and the contribution of direct sunlight was strongly reduced in particular toward shorter wavelengths as expected from increased scattering.

[19] Regarding photolysis frequencies, Figure 6 (left) shows diurnal variations of $j(O^1D)$ and $j(NO_2)$ on 15 July 2003. The wavelength ranges of the corresponding photolysis processes (Table 1) resulted in the different shapes of the diurnal variations and the different contributions of direct sunlight. The relative diurnal variations of other photolysis frequencies (except $j(NO_3)$) ranged within these extremes.

[20] In the presence of clouds the situation was obviously more complex in particular under conditions with broken cloud cover and occasional direct sunlight. Figure 6 (right) shows examples from 18 July 2003. Here diffuse sky radiation was temporarily increased by reflections of direct sunlight in clouds. On the other hand, direct sunlight was sporadically blocked by clouds. Consequently, photolysis frequencies were higher or lower compared with clear-sky conditions but lower values were more common. Because of the higher contribution of direct sunlight, these cloud effects were more pronounced for $j(NO_2)$ than for $j(O^1D)$. Under overcast conditions photolysis frequencies were always lower compared with clear-sky conditions at the same time of day. Nevertheless, there were strong and also rapid variations upon changes in cloud thickness (see section 3.2.1).

3.1.2. Comparison of Field Sites Above the Forest

[21] The cloud effects discussed in section 3.1.1 were local and could have affected the measurement sites above the forest differently at a horizontal distance of 370 m (distance tower roof). However, a comparison with the additional above forest filter radiometer measurements of $j(NO_2)$ and $j(O^1D)$ at the tower [*Bohn et al.*, 2006] showed that the roof measurements were a reasonable reference for the forest site. Figure 7 shows correlations of $j(NO_2)$ obtained at the two sites for the complete campaign periods in 2002 and 2003. The correlations were excellent in both years with more than 96% of data similar within 20%. For $j(O^1D)$ a similar result was obtained.

3.2. Forest Measurements

3.2.1. Overcast Conditions

[22] Figure 8 (left) shows variations of photolysis frequencies $j(O^1D)$ and $j(NO_2)$ on 1 July 2002 above the forest and at the ground from positions clearing 1 and forest 1. Conditions on this day were completely overcast. However, there were considerable, sometimes rapid variations in the course of the day. These variations were observed simultaneously at the clearing and forest positions. Plots of photolysis frequencies from these positions as a function of above forest values are shown in Figure 8 (right). As mentioned in section 2.1.2, data sets were synchronized by linear interpolations for this comparison. This procedure

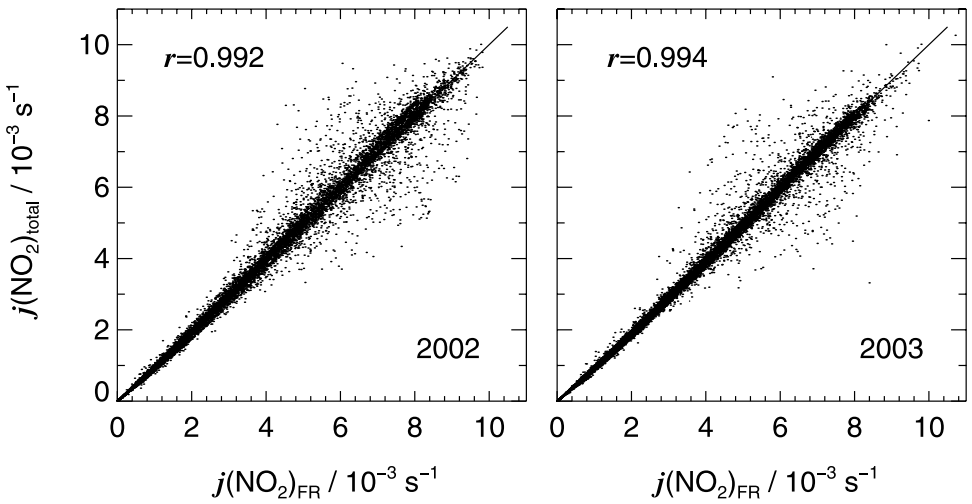

Figure 7. Comparison of above forest measurements of $j(NO_2)$ with a filter radiometer at the ECHO main tower (FR) and the spectroradiometer at the roof site (SR 2, total) at a distance of 370 m. Data for the complete campaign periods of (left) 2002 and (right) 2003 are shown, $N = 13{,}700$ (2002), $N = 14{,}200$ (2003).

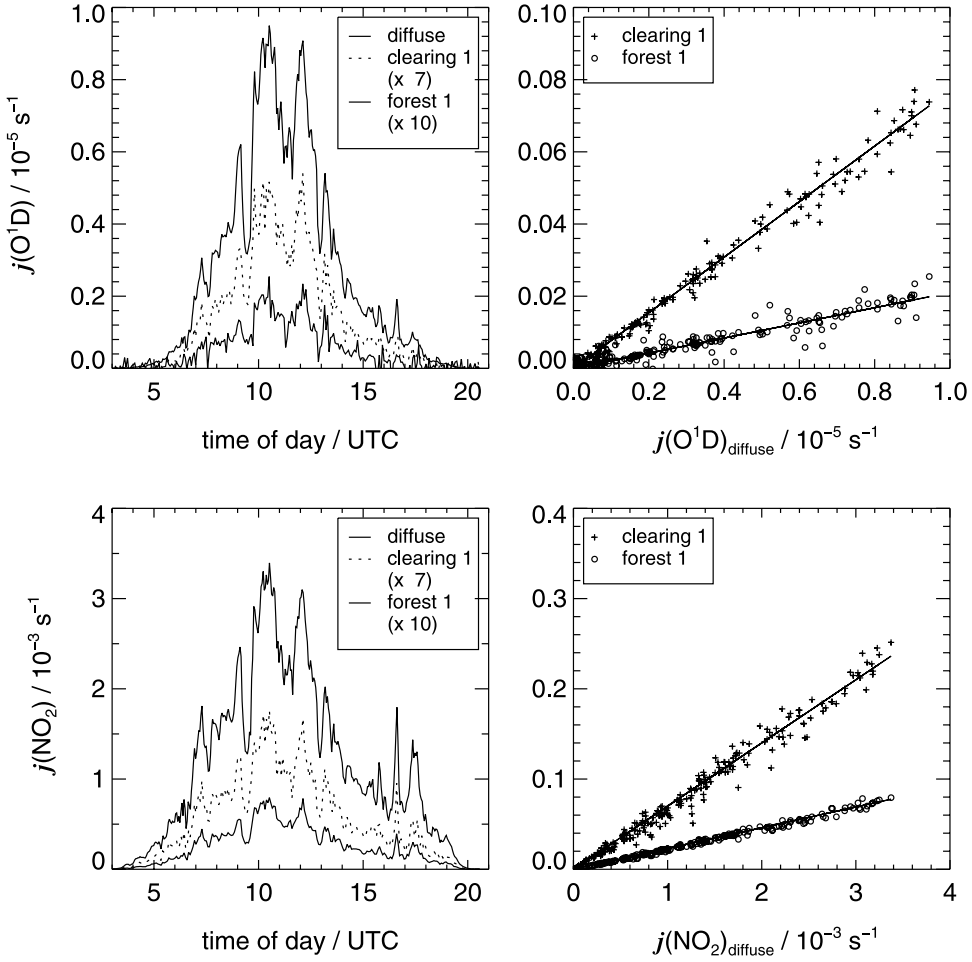

Figure 8. (left) Diurnal variations of $j(O^1D)$ and $j(NO_2)$ on 1 July 2002 (overcast conditions) above the forest (diffuse equals total), and at positions clearing 1 and forest 1 (from top to bottom). Note that the curves for clearing 1 and forest 1 were scaled by factors 7 and 10, respectively. (right) Correlations of forest and clearing data with above forest data. Solid lines indicate linear regressions with slopes of 0.021 (forest) and 0.077 (clearing) for $j(O^1D)$ and 0.023 (forest) and 0.070 (clearing) for $j(NO_2)$.

Table 3. Linear Correlation Coefficients r and Mean Ratios f of Photolysis Frequencies Relative to Above Forest Values Under Overcast Conditions[a]

Position	Process	N	r	f
		2002		
Forest 1	$j(NO_2)$	617	0.985	0.022 ± 0.002
	$j(O^1D)$	317	0.941	0.021 ± 0.007
Forest 2	$j(NO_2)$	743	0.970	0.010 ± 0.002
	$j(O^1D)$	128	0.837	0.011 ± 0.007
Clearing 1	$j(NO_2)$	634	0.950	0.067 ± 0.010
	$j(O^1D)$	442	0.965	0.070 ± 0.010
Clearing 2	$j(NO_2)$	812	0.965	0.072 ± 0.013
	$j(O^1D)$	511	0.965	0.074 ± 0.013
		2003		
Forest 3a	$j(NO_2)$	601	0.968	0.024 ± 0.004
	$j(O^1D)$	313	0.958	0.026 ± 0.006
Forest 3b	$j(NO_2)$	589	0.964	0.015 ± 0.002
	$j(O^1D)$	266	0.900	0.020 ± 0.015
Forest 4	$j(NO_2)$	537	0.980	0.019 ± 0.002
	$j(O^1D)$	256	0.963	0.021 ± 0.005
	$j(NO_3)_r$	365	0.961	0.022 ± 0.005
	$j(NO_3)_m$	329	0.928	0.021 ± 0.004
Clearing 2	$j(NO_2)$	557	0.961	0.061 ± 0.011
	$j(O^1D)$	381	0.971	0.067 ± 0.015
	$j(NO_3)_r$	383	0.910	0.062 ± 0.014
	$j(NO_3)_m$	350	0.924	0.062 ± 0.014
		ECHO Site (Typical)[b]		
Forest	all	–	–	0.02 ± 0.01
Clearing	all	–	–	0.07 ± 0.02

[a]Conditions are ~8 days in 2002 and ~6 days in 2003. Data were not considered where $j(NO_2) \leq 1 \times 10^{-6} s^{-1}$ and $j(O^1D) \leq 5 \times 10^{-8} s^{-1}$ at the forest sites, respectively. Error bars are 1σ.
[b]The data were considered typical values for the ECHO forest and clearing under overcast conditions.

may have introduced scatter in addition to possible local differences discussed in section 3.1. Nevertheless, the dependencies were linear in good approximation and similar slopes were derived for $j(O^1D)$ and $j(NO_2)$.

[23] Corresponding results were obtained on other overcast days and for other forest and clearing positions. Table 3 shows a summary of linear correlation coefficients and mean ratios f of photolysis frequencies for all positions from selected overcast days within the different campaign periods. The selection criterion was that on these days measurements with and without shadow ring above the forest were similar within the measurement uncertainties. The ratios of Table 3 were summarized to typical attenuation factors $f = 0.02 \pm 0.01$ for the forest surrounding the ECHO tower and $f = 0.07 \pm 0.02$ for the clearing that hosted the tower. These attenuation factors applied for all photolysis frequencies including $j(NO_3)$ (data from 2003 campaign only).

[24] A linear relationship between above and below canopy spectral actinic flux and photolysis frequencies under overcast conditions was not surprising because the angular distribution of UV sky radiance is usually independent of time and wavelength in good approximation [*Grant and Heisler*, 1997]. Moreover, similar attenuation factors for different photolysis frequencies pointed toward a wavelength-independent attenuation of actinic flux by the forest. Figure 9 shows actinic flux spectra and ratios of spectra on 17 August 2003 under overcast conditions. This day was selected because the diode array spectroradiometer was operative providing above forest data up to 700 nm. Except for few wavelength positions, measurements of SR 2 (total), SR 2 (diffuse) and SR 3 (diode) above the forest agreed within about 5%. Below 550 nm structures of the spectra were reproduced more precisely by the scanning instruments SR 1 (forest) and SR 2 (roof) because of higher spectral resolutions. This explained the higher scatter of the ratios SR 1/SR 3 in this wavelength range. Spectral resolutions of SR 1 and SR 3 were comparable above 550 nm and consequently the scatter was reduced in this range.

[25] In general the ratios were fairly constant up to 700 nm. In a range 500–650 nm ratios were slightly increased with maxima around 550 nm about 25% (forest) and 10% (clearing) above the means below 500 nm, respectively. The constant ratios below about 500 nm explain the similar attenuation factors for $j(NO_2)$ and $j(O^1D)$ in Table 3. Although $j(NO_3)$ was affected by the increased fluxes around 550 nm, the integrated effect was not significant within the error limits. At wavelengths above 700 nm actinic flux increased strongly at the forest and the clearing locations. This can be explained by an increased transmission of the foliage. However, no photochemical effect was associated with this increase.

3.2.2. Clear-Sky and Broken Cloud Conditions

[26] Figure 10 shows diurnal variations of photolysis frequencies $j(O^1D)$ and $j(NO_2)$ on a clear-sky day (15 July 2003) above the forest and at positions clearing 2 and forest 4. Above canopy data of this day were already discussed in section 3.1.1. Below canopy data also exhibited smooth diurnal variations except for sporadic sharp peaks associated with direct sunlight incident through gaps in the foliage. These gaps must have been small compared to the apparent size of the Sun's disk because the amplitudes of the peaks were much smaller than the contribution of direct sunlight above canopy (mind the

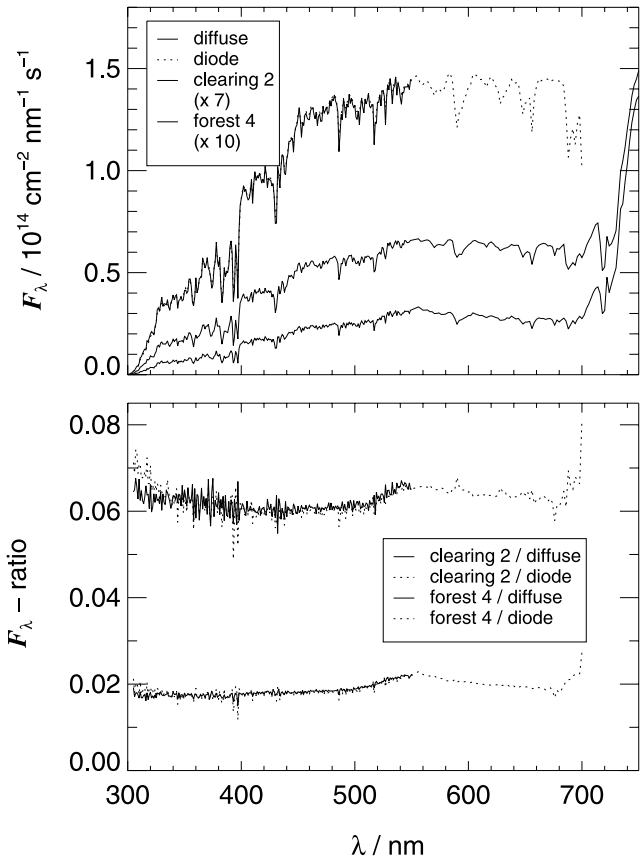

Figure 9. (top) Actinic flux spectra obtained on 17 August 2003 at around noon under overcast conditions above the forest (diffuse equals total, and diode), and at positions clearing 2 and forest 4, scaled by factors 7 and 10, respectively (from top to bottom). (bottom) Ratios of spectra from Figure 9 (top).

different scales in Figure 10), i.e., they were caused by penumbra. Accordingly it was found that the peak patterns changed from day to day. Moreover, within the scanning time of a spectrum (~4.5 min) the Sun was covering a distance about twice its apparent diameter of 0.5°. This further reduced the amplitudes of peaks from gaps smaller than about 1° and produced differences in the peak patterns for $j(O^1D)$ and $j(NO_2)$ caused by differences in measurement times and periods. Measurement periods for $j(NO_2)$ were longer by a factor of ~3 compared to $j(O^1D)$. In addition, there may have been momentary changes of the gap patterns induced by wind movements of branches and leaves. In any case, peak heights for $j(O^1D)$ were usually lower because of the smaller contribution of direct sunlight above the forest.

[27] Similar to Figure 8, Figure 10 (right) shows forest and clearing data plotted as a function of the diffuse part of above forest photolysis frequencies. As in the case of overcast conditions and except for few outliers produced by the peaks, there was a linear relationship between the data in good approximation. However, compared with overcast conditions (Figure 8 and dashed lines in Figure 10), the slopes were significantly smaller in particular for the clearing. Moreover, the differences appeared larger for $j(NO_2)$ where also a nonlinearity and hysteresis were recognizable for the clearing data. These differences between overcast and clear-sky conditions could not be attributed to direct sunlight transmitted through the foliage. If a significant fraction of direct sunlight were transmitted permanently, the slopes would be larger rather than smaller compared with overcast conditions. Thus the effect was most likely caused by differences in the angular distributions of diffuse sky radiation under clear-sky conditions. This hypothesis is addressed in more detail in section 3.4.

[28] Figure 11 shows actinic flux spectra and ratios of spectra from another clear-sky day (19 July 2003) where the diode array spectroradiometer was operative. The period for the comparison corresponded to local noon conditions on that day (χ = 29°) and contained no obvious peaks caused by direct sunlight passing through gaps in the foliage. Spectral actinic flux ratios with regard to diffuse sky radiation above the forest were again constant below about 500 nm in good approximation. The most obvious differences compared with Figure 9 were lower ratios below 500 nm and a stronger increase above 500 nm caused by a transmission of direct sunlight by the foliage that was not attributable to gaps. A comparison of the maximum increase at 550 nm with above canopy direct sunlight implied an effective transmittance of the foliage of no more than about 0.5% around 550 nm.

[29] Literature data indeed show increased transmittances of mature summer season beech leaves of 8–15% around 550 nm [*Eller et al.*, 1981; *Tanner and Eller*, 1986]. Arithmetically, the estimated 0.5% transmittance thus corresponded to passage through 2.1–2.8 leaves. However, light transmission through leaves is diffuse. The increased flux around 550 nm may therefore have come from illuminated foliage in any direction. Nevertheless, this estimate explained that leaf transmittances of around 1% as reported for 400 nm [*Eller et al.*, 1981; *Tanner and Eller*, 1986] were not detectable.

[30] The ratios with regard to total actinic flux above the forest were generally decreasing with wavelength up to about 700 nm. Except for the short periods when direct sunlight was received through gaps, the ratios were much smaller compared with overcast conditions. Whether or not this result was applicable for the forest as a whole is discussed in section 3.4. Mean ratios as in Table 3 were not calculated for clear-sky conditions because of the sporadic influence of peaks and obvious nonlinearities.

[31] Days with broken cloud cover showed a behavior in between the extremes described so far. At relatively low cloud cover a clear-sky behavior as in Figure 10 prevailed (e.g., on 18 July 2003, Figure 6) while with increasing cloud cover, ratios increased to values typical for overcast conditions.

3.3. Analysis of Sky Photographs: Canopy Gap Fractions

[32] The results obtained so far were consistent with the foliage being virtually opaque toward radiation at wavelengths below about 500 nm. Thus the simplest perception of transfer of radiation within the forest in this wavelength range is either absorption by the foliage or transmission through gaps. It should be noted that this concept is by no means new and has for example been implemented in instruments for radiometric measurements of LAIs (e.g.,

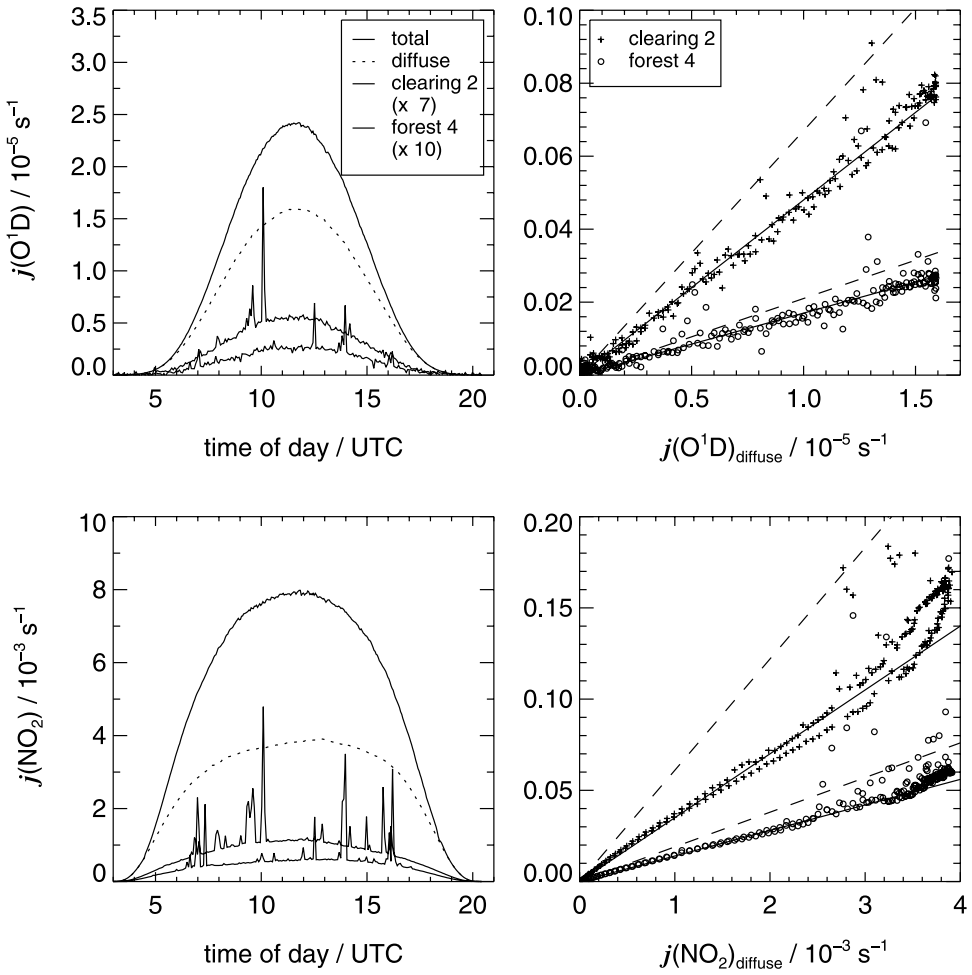

Figure 10. (left) Diurnal variations of $j(O^1D)$ and $j(NO_2)$ on 15 July 2003 (clear-sky conditions) above the forest (total and diffuse) and at positions clearing 2 and forest 4 (from top to bottom). Note that the curves for clearing 2 and forest 4 were scaled by factors 7 and 10, respectively. (right) Correlations of forest and clearing data with the diffuse fraction of above forest data. Solid lines indicate approximate linear relationships neglecting outliers caused by direct sunlight with slopes of 0.017 (forest) and 0.052 (clearing) for $j(O^1D)$ and 0.014 (forest) and 0.035 (clearing) for $j(NO_2)$. Dashed lines indicate the results from overcast conditions (Table 3) for comparison.

Licor, LAI-2000). Consequently, the distribution of gaps was an essential parameter also determining the actinic flux received at a given location.

[33] In Figures 3 and 4, two examples of sky photographs from the ECHO site were shown. At each forest position, photographs were taken during summer and winter seasons. After digitalization these photographs were converted to gray scale and finally black and white images. From these images the fractions of visible sky, denoted canopy gap fractions α in the following, as a function of polar angle ϑ were derived by binning and averaging the data regardless of azimuth angles. The conversion to black and white images was made by varying the gray scale limits between black and white until the measured attenuation factors f of Table 3 were obtained for the different locations upon integration (see equation (7) for comparison):

$$f = \int_0^{2\pi} \int_0^{\pi/2} \alpha(\vartheta) L(\vartheta) \sin(\vartheta) \mathrm{d}\vartheta \mathrm{d}\varphi \qquad (8)$$

For the winter images a measured attenuation factor $f = 0.33$ was used [*Bohn et al.*, 2006]. Calculations were made numerically using a standard overcast (SOC) sky radiance distribution [*Grant and Heisler*, 1997] after 2π-sr normalization:

$$L(\vartheta) = \frac{1 + b\cos(\vartheta)}{\pi(2+b)} \qquad b = 1.23 \qquad (9)$$

This distribution is an empirical description of measured radiances under overcast conditions which can be used in the UV and VIS range in good approximation [*Grant and Heisler*, 1997].

[34] It should be noted that this analysis of the photographs was considered semiquantitative because the camera did not monitor UV radiation. Moreover, the relationship between brightness and radiance in the photographs was not necessarily linear and may also have depended on polar angle. The idea behind this was that gaps were much

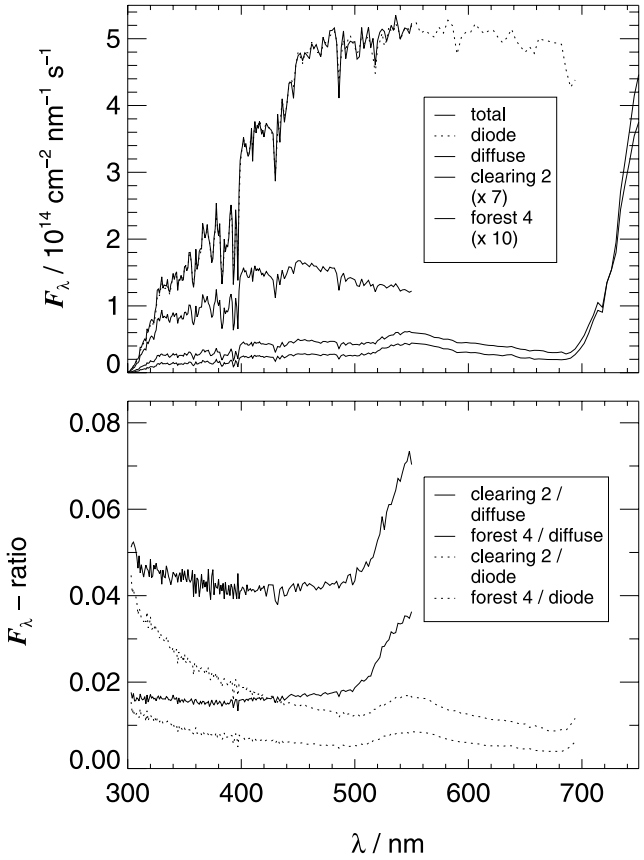

Figure 11. (top) Actinic flux spectra obtained on 19 July 2003 around noon under clear-sky conditions above the forest (total, diode, and diffuse) and at positions clearing 2 and forest 4, scaled by factors 7 and 10, respectively (from top to bottom). (bottom) Ratios of spectra from Figure 11 (top).

brighter than foliage allowing a proper distinction also assignable to the UV.

[35] Figure 12 shows canopy gap fractions obtained for the different positions and seasons. During the winter season (Figure 12, top left), i.e., in the absence of foliage, the results looked comparable for the different forest positions and the clearing, except for areas close to the zenith ($\vartheta \leq 30°$). For comparison, above forest conditions for all seasons ($\alpha = 1$) were also indicated.

[36] During summer (Figure 12, top right) the α were strongly reduced by the foliage. Moreover, the results for the different forest sites were very different despite averaging over azimuth angles. This confirmed the impression of strong irregularity evident in Figure 3. The only similarity with the winter data was that sites with low α at small polar angles during the winter season exhibited extremely low α in the same area during the summer season. This was consistent with the site being situated underneath the crown of a tree. The summer data from the clearing increased strongly at $\vartheta \leq 30°$ (also shown in Figure 12 (left) for clarity). Upon weighting the data with $\sin(\vartheta)$ according to equation (8), differences between the forest and the clearing became insignificant during the winter season (Figure 12, middle left). The dashed curve approaching unity at $\vartheta = 90°$ again indicates above forest conditions explaining the strong reduction of photolysis frequencies during the winter season by effective obstruction of the sky at large polar angles. Despite slightly decreasing radiances with increasing polar angle (equation (9)) this explained the strong attenuation $f \approx 0.33$ already during the winter season.

[37] For the summer season weighting with $\sin(\vartheta)$ (Figure 12, middle right) harmonized the overall impression but there were significant differences remaining between the sites. Moreover, in contrast to winter conditions, the clearing site benefited strongly from the gap in the foliage close to the zenith explaining the increased photolysis frequencies compared with the forest sites.

[38] Figure 12 (bottom) indicates the differences between actinic flux and irradiance by weighting α with the product $\sin(\vartheta)\cos(\vartheta)$ (see equation (6)). Here the relative ϑ dependence of radiance reception was more comparable to above forest conditions because the importance of large polar angles was diminished by the factor $\cos(\vartheta)$. Therefore, compared to actinic flux, attenuation of irradiance was probably less effective and less dependent on the angular distribution of radiance. On the basis of the data of Figure 12, scaling factors for irradiance under overcast conditions were estimated 20–30% greater than for actinic flux. However, no measurements of spectral irradiance were made during the ECHO project.

3.4. Application of Model Gap Fractions

[39] The dotted curves in Figure 12 (right) show a rough mean of canopy gap fractions for the forest sites by fitting a parameterization as a function of polar angle:

$$\alpha(\vartheta)_{\text{forest}} = 0.027\exp\left(-5.0(\vartheta/\text{rad} - 0.57)^{4.9}\right) \qquad (10)$$

The coefficient was chosen to meet the mean attenuation factor $f = 0.02$ (Table 3). For the clearing a similar approach was used to produce an analytical description for summer conditions (see dotted curves in Figure 12 (left)):

$$\alpha(\vartheta)_{\text{clearing}} = \alpha(\vartheta)_{\text{forest}} + 0.97 \cdot \exp\left(-11.5(\vartheta/\text{rad} - 0.02)^{2.0}\right) \qquad (11)$$

The mean canopy gap fractions described by equations (10) and (11) were used to investigate their effect on analytical clear-sky radiance distributions of diffuse sky radiation from literature to reproduce the differences observed between overcast and clear-sky conditions. The day 15 July 2005 was again taken as an example. In Figure 13, forest and clearing data are shown together with modeled data based on photolysis frequencies measured above the forest. The dashed lines were calculated using clear-sky UV-A and UV-B radiance distributions by *Grant et al.* [1997] for the calculation of $j(NO_2)$ and $j(O^1D)$, respectively. For example, the following equation was used for the calculation of $j(O^1D)$ in the forest:

$$j(O^1D)_{\text{forest,diff}} = j(O^1D)_{\text{diffuse}} \cdot \int_0^{2\pi}\int_0^{\pi/2} \alpha(\vartheta)_{\text{forest}} L(\vartheta,\varphi)\sin(\vartheta)\,d\vartheta\,d\varphi \qquad (12)$$

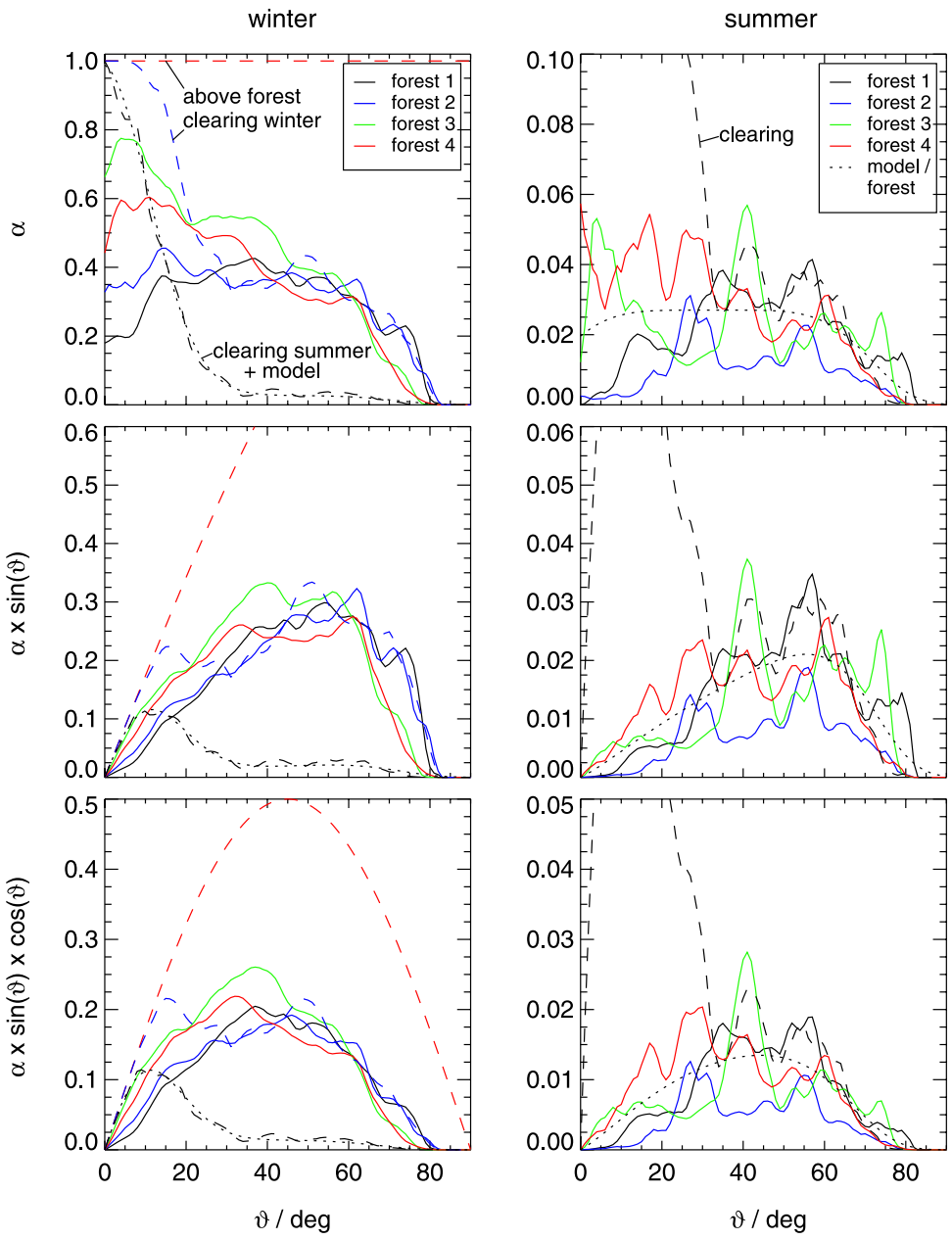

Figure 12. Results of fish-eye photograph analysis. (top) Canopy gap fraction α as a function of polar angle ϑ at winter and summer seasons for the different forest sites (solid lines) and the clearing (dashed lines). The clearing results for the summer season (indicated by dashed lines) are shown for clarity. The dashed line in Figure 12 (left) at $\alpha = 1$ indicates above forest conditions. (middle and bottom) Same as Figure 12 (top) but for the products $\alpha \sin(\vartheta)$ contributing to actinic flux and $\alpha \times \sin(\vartheta)\cos(\vartheta)$ contributing to irradiance, respectively (see text). Dotted curves show rough mean dependencies of α for (left) the clearing and (right) forest positions (equations (10) and (11)).

In this equation, $L(\vartheta,\varphi)$ is the analytical (2 π-sr normalized) UV-B sky radiance distribution by *Grant et al.* [1997]. For the clearing, a corresponding equation applies by using $\alpha_{clearing}$ instead of α_{forest} while for $j(NO_2)$ the UV-A radiance distribution by *Grant et al.* [1997] was applied.

[40] The agreement between measured and modeled data in Figure 13 was satisfactory given the simplicity of the approach. Moreover, Figure 13 (right) shows that compared with overcast conditions the effects observed for clear-sky conditions could be reproduced, namely, lower ratios, a nonlinearity for the clearing data and a more pronounced effect for $j(NO_2)$ (UV-A) than for $j(O^1D)$ (UV-B) (see Figure 10). Thus these effects were related with the differences in sky radiance distributions and the confined fields of view at forest and clearing positions. The dashed lines in Figure 13 (right) were calculated using the SOC radiance distribution of equation (9) and therefore correspond to the mean attenuation factors given in Table 3.

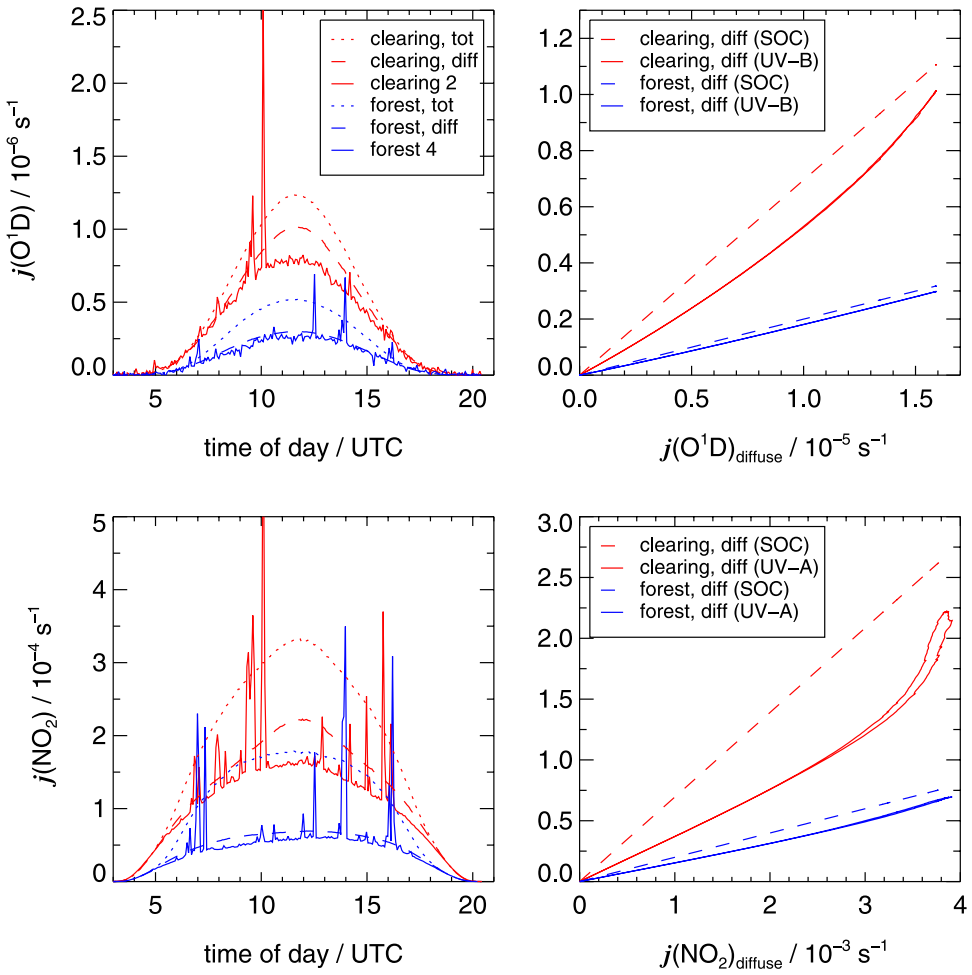

Figure 13. (left) Diurnal variations of $j(O^1D)$ and $j(NO_2)$ on 15 July 2003 (clear-sky conditions) at clearing position 2 (upper curves) and forest position 4 (lower curves). Dashed lines show the results of a model approach using above forest photolysis frequencies from diffuse sky radiation (equation (12)). Dotted lines indicate the expected behavior including direct sunlight (equation (13)). (right) Correlations of measured and modeled data according to equation (12). Dashed lines indicate the result under overcast conditions.

[41] The dotted curves in Figure 13 (left) indicate the mean total photolysis frequencies expected from diffuse and direct contributions, e.g., for $j(O^1D)$:

$$j(O^1D)_{forest,tot} = j(O^1D)_{forest,diff} + j(O^1D)_{direct}\alpha(\chi)_{forest} \quad (13)$$

A comparison of modeled and measured total photolysis frequencies showed that the mean effect of direct sunlight was overestimated by the model. However, this could be explained by the strong variability of the size of the gaps also evident in Figure 3. The diffuse sky radiation incident at a forest position seemed to be dominated by a number of relatively large gaps. The chance that the Sun moved across one of these large gaps was small for a selected location but there were other, few locations in the vicinity where this happened (Sun flecks). If at these locations the Sun was fully visible, the actinic flux was increased very strongly, e.g., by a factor of ~30 for $j(NO_2)$ at around noon. Because this increase affected only confined areas at a time, it remained mostly unobserved. However, the average effect of these bright regions for the forest mean of the photolysis frequencies must have been significant and should be described correctly by equation (13).

[42] On the basis of the model calculations, the integrated, daily fractions of photolysis frequencies $j(O^1D)$ and $j(NO_2)$ received on average at forest and clearing locations were summarized in Table 4 for 15 July 2003. The fractions of photolysis frequencies from diffuse sky radiation were slightly smaller compared with overcast conditions, as expected from Figure 13 (right). The fractions from direct sunlight were similar for clearing and forest positions because in the model treatment the clearing did not receive direct radiation through the main gap in the canopy. Of course, this was only true for the clearing close to ground level. The fractions of total actinic flux for the clearing were different for $j(O^1D)$ and $j(NO_2)$, and also differed significantly from the mean result under overcast conditions (f = 0.07, Table 3). However, for the forest the overall effect was very similar for $j(O^1D)$, $j(NO_2)$ and compared with overcast conditions. Thus a mean attenuation factor f = 0.02 applied for all conditions close to ground level in

Table 4. Integrated, Modeled Daily Fractions of Photolysis Frequencies Calculated for the Forest and the Clearing 2 m Above Ground With Regard to Above Forest Data on 15 July 2003 (Clear-Sky)[a]

	Clearing		Forest	
	$j(O^1D)$	$j(NO_2)$	$j(O^1D)$	$j(NO_2)$
Diffuse	0.057	0.047	0.018	0.017
Direct	0.027	0.025	0.027	0.025
Total	0.048	0.037	0.021	0.021

[a]On this day the integrated above forest fractions of diffuse sky radiation were 0.70 and 0.54 for $j(O^1D)$ and $j(NO_2)$, respectively.

good approximation. Seasonal changes affecting the maximum elevation of the Sun and the contributions of direct sunlight above the forest were not considered.

3.5. Implications for the ECHO Site Photochemistry

[43] Profile measurements of photolysis frequencies in the forest showed that photolysis frequencies dropped rapidly within about 5 m below canopy top followed by a more gradual reduction toward the ground [*Bohn et al.*, 2006]. On average 4% of above forest values were found in a range below about 28 m. Thus the measurements of this work, collected at forest and clearing sites close to ground level were in a range representative for the bulk of the forest.

[44] An important issue regarding the chemistry within the forest is what fraction of reactive BVOCs emitted by plants is injected into the boundary layer and what fraction is already converted within the forest by reactions with OH, NO_3 and O_3 [e.g., *Makar et al.*, 1999; *Stroud et al.*, 2005]. At the ECHO site the principal reactive BVOC was isoprene that was emitted during daytime by oak trees in the surrounding forests. Typical maximum concentrations were 2–4 ppbV in the early afternoon [*Spirig et al.*, 2005]. Because OH concentrations were found to be linearly correlated with photolysis frequencies, degradation of isoprene by OH within the forest was estimated negligible except for residence times exceeding about one hour [*Bohn et al.*, 2006]. Within the canopy there may have been an active zone characterized by increased actinic fluxes, strong emissions and slow transport caused by dense foliage but this layer had a very limited extension of a few meters.

[45] In contrast to OH, daytime NO_3 radical concentrations could have been increased below canopy as a result of reduced photolysis frequencies and reduced NO concentrations from NO_2 photolysis. In a first step, the photostationary equilibrium of NO, NO_2 and O_3 on 15 July 2005 was examined. At around noon on that day, O_3 and NO_x levels were about 50 ppbV and 1.5 ppbV, respectively (F. Rohrer, private communication, 2005). Considering photolysis of NO_2 (equations (3) and (4)) and reaction of NO with O_3,

$$O_3 + NO \rightarrow O_2 + NO_2 \tag{14}$$

photostationary state (PS) concentrations of NO were calculated using

$$[NO]_{PS} = \frac{[NO_x]j(NO_2)}{[O_3]k_{14} + j(NO_2)} \tag{15}$$

Taking an above forest photolysis frequency $j(NO_2)$ of 8×10^{-3} s^{-1}, $[NO]_{PS}$ = 390 pptV was obtained (T = 298 K, p = 1000 hPa, $k_{14} = 1.9 \times 10^{-14}$ cm^3 s^{-1} [*Sander et al.*, 2003]). For the clearing and forest positions concentrations of 19 pptV and 10 pptV were calculated, using $j(NO_2) = 3.0 \times 10^{-4}$ s^{-1} and 1.6×10^{-4} s^{-1}, respectively (modeled mean $j(NO_2)$ of Figure 13). Thus the concentration of NO was expected to be reduced substantially within the forest. Measurements on 15 July 2005 showed significantly lower NO concentrations above the canopy (~50 pptV) and NO concentrations in reasonable agreement with the PS estimate 9 m above ground at the tower (~30 pptV) (F. Rohrer, private communication, 2005). The discrepancy above the forest was explainable qualitatively by the presence of RO_2 and HO_2 radicals and possibly transport processes diminishing the differences between above and below canopy conditions close to canopy top.

[46] With regard to NO_3, photostationary state concentrations were estimated considering the following reactions:

$$O_3 + NO_2 \rightarrow O_2 + NO_3 \tag{16}$$

$$NO_3 + NO_2 \rightarrow N_2O_5 \tag{17}$$

$$N_2O_5 \rightarrow NO_2 + NO_3 \tag{18}$$

$$NO_3 + C_5H_8 \rightarrow \text{products} \tag{19}$$

$$NO_3 + C_{10}H_{16} \rightarrow \text{products} \tag{20}$$

$$NO_3 + NO \rightarrow 2NO_2 \tag{21}$$

$$NO_3 + h\nu \rightarrow NO_2 + O(^3P)(\rightarrow NO_2 + O_3) \tag{22}$$

$$NO_3 + h\nu \rightarrow NO + O_2 \tag{23}$$

Formation of N_2O_5 and its reaction back to NO_3 (equations (17) and (18)) cancelled out in the PS approach. Reaction with isoprene (C_5H_8) and monoterpenes ($C_{10}H_{16}$) (equations (19) and (20)) were assumed the major loss processes for NO_3 in addition to reaction with NO (equation (21)) and photolysis (equations (22) and (23)). The photolyses of NO_3 were accounted for by a combined rate constant $j(NO_3)$. $[NO_3]_{PS}$ was then given by

$$[NO_3]_{PS} = \frac{([NO_x] - [NO]_{PS})[O_3]k_{16}}{j(NO_3) + [NO]_{PS}k_{21} + [C_5H_8]k_{19} + [C_{10}H_{16}]k_{20}} \tag{24}$$

For the O_3 + NO_2 reaction a rate constant $k_{16} = 3.2 \times 10^{-17}$ cm^3 s^{-1} was used (298 K [*Sander et al.*, 2003]). For $j(NO_3)$ measured data on 19 July 2003 above the forest (Table 1) and similar attenuation factors as for $j(NO_2)$ were used. For $[NO]_{PS}$ calculated and measured concentrations were inserted and $k_{21} = 2.6 \times 10^{-11}$ cm^3 s^{-1} (298 K [*Sander et al.*, 2003]). Isoprene and total monoterpene concentrations were about 2.3 and 0.25 ppbV around noon on 15 July 2003 [*Spirig et al.*, 2005]. For isoprene a rate constant $k_{19} = 7.0 \times 10^{-13}$ cm^3 s^{-1} was used [*Atkinson and Arey*, 2003]. Because different monoterpenes could not be distinguished by the

Table 5. Results of Photostationary State Calculations of NO and NO_3 Concentrations on 15 July 2003 According to Equations (15) and (24)[a]

	Above Forest	Clearing	Forest
$j(NO_2)$, 10^{-3} s^{-1}	8.0	0.30	0.16
$[NO]_{PS}$, pptV	385 (50)[b]	19 (30)[c]	10 (30)[d]
$j(NO_3)$, 10^{-2} s^{-1}	19	0.71	0.38
$[NO_3]_{PS}$, pptV	0.08 (0.18)	0.49 (0.46)	0.53 (0.47)

[a]$[O_3]$ = 50 ppbV, $[NO_x]$ = 1.5 ppbV, $[C_5H_8]$ = 2.3 ppbV (isoprene), $[C_{10}H_{16}]$ = 0.25 ppbV (monoterpenes). NO_3 concentrations in parentheses were calculated using measured NO concentrations given in parentheses. $[NO_3]$ = 0.59 pptV was obtained for darkness assuming [NO] = 0 and $j(NO_3)$ = 0.
[b]Measured NO above forest.
[c]Measured NO at clearing tower (9 m).
[d]Estimated maximum NO in forest.

detection method of *Spirig et al.* [2005], a mean rate constant $k_{20} = 1.0 \times 10^{-11}$ cm^3 s^{-1} was estimated [*Atkinson and Arey*, 2003]. With this assumption about 60% of the BVOC reactivity with regard to NO_3 was attributable to the monoterpenes. Calculated NO_3 concentrations are listed in Table 5. They ranged around 0.1 pptV above canopy and 0.5 pptV below canopy. Unfortunately, these concentrations could not be confirmed experimentally because they were well below the detection limit of about 1 pptV for NO_3 radicals during the ECHO campaign (D. Mihelcic, private communication, 2005).

[47] With the calculated NO_3 concentrations of Table 5, and the measured concentrations of isoprene and monoterpenes noted above, loss rates L/pptV h^{-1} were calculated for above and below canopy conditions. For isoprene these results ranged between 10–25 pptV h^{-1} above canopy and 65–75 pptV h^{-1} below canopy. For the monoterpenes the corresponding loss rates were 20–40 pptV h^{-1} above canopy and 100–120 pptV h^{-1} below canopy. For comparison, similar estimates were made for the loss rates by reactions with OH and O_3. For OH a measured above forest concentration of 0.2 pptV was used (A. Hofzumahaus, private communication, 2005). Because OH concentrations correlated linearly with $j(O^1D)$, the mean scaling factor of 0.04 noted above was applied to estimate a mean OH concentration below canopy. O_3 concentrations were assumed similar within and above the forest.

[48] The calculated loss rates for the reactants NO_3, OH, and O_3 are listed in Table 6. For isoprene reactions with NO_3 and O_3 accounted for 20% and 35% of the total loss in the forest compared with 0.4% and 3% above the forest. However, the total loss rate was only 8% of the above forest value. On the other hand, for the monoterpenes the total loss rate below canopy was 40% of the above forest value because the effect of reduced OH was partly compensated by the increased NO_3 concentration. 46% of the monoterpene loss in the forest was attributable to the NO_3 reaction.

[49] To estimate the importance of the calculated loss rates for a potential in-forest degradation, BVOC flux data by *Spirig et al.* [2005] were consulted. Isoprene and monoterpene fluxes at the ECHO tower reached maxima of about 1.0 and 0.3 μg m^{-2} s^{-1} on 15 July 2003. These fluxes were compared to the BVOC loss rates using a mean forest height of 28 m below canopy. This revealed that no more than about 0.8% of isoprene and 3.4% of monoterpenes were processed within the forest. These low fractions were consistent with in-forest residence times of BVOCs of the order 2–3 min that were obtained by comparing the BVOC fluxes with the BVOC inventories below canopy as reported by *Spirig et al.* [2005].

[50] In conclusion, chemistry in the forest at the ECHO site was probably too slow for a significant reduction of net emissions of isoprene and monoterpenes into the boundary layer. However, the situation might have been different for compounds with exceptionally fast rate constants with regard to NO_3 or O_3. Moreover, the relative importance of NO_3 was probably increased toward the morning and the evening when BVOC concentrations and fluxes were lower. More detailed studies considering composition, chemistry and transport are therefore needed to assess the roles of NO_3 and O_3 as daytime reactants within forests.

4. Conclusions

[51] Spectral actinic flux measurements in a deciduous forest at the ECHO field site indicated strongly reduced photolysis frequencies close to ground level. About 2% of

Table 6. Rate Constants k for Reactions of Isoprene and Monoterpenes With NO_3, OH and O_3, Estimated and Measured Concentrations c of NO_3, OH, and O_3 Above and Below Canopy, and Estimated Loss Rates L of Isoprene and Monoterpenes With Regard to Reactions With NO_3, OH, and O_3 at Concentrations of 2.3 ppbV (Isoprene) and 0.25 ppbV (Monoterpenes), Respectively

		Reactant		
Location	Quantity	NO_3	OH	O_3
	k (isoprene)[a], cm^3 s^{-1}	7.0×10^{-13}	1.0×10^{-10}	1.3×10^{-17}
	k (monoterpene),[b] cm^3 s^{-1}	1.0×10^{-11}	1.0×10^{-10}	1.0×10^{-16}
Above canopy	c, pptV	0.08–0.18[c]	0.2[d]	5×10^{4}[f]
Below		0.46–0.53[c]	0.008[e]	5×10^{4}[f]
Above canopy	L (isoprene), pptV h^{-1}	10–25	4200	130
Below		65–75	170	130
Above canopy	L (monoterpene), pptV h^{-1}	20–40	450	110
Below		100–120	20	110

[a]*Atkinson and Arey* [2003].
[b]*Atkinson and Arey* [2003], estimated mean for monoterpenes.
[c]See Table 5.
[d]Typical value, measured on 19 July 2003.
[e]Estimated mean by scaling above canopy concentration.
[f]Measured on 15 July 2003.

above forest values were obtained for all relevant photolysis processes under all conditions. In the tower clearing the situation was more complex with attenuation factors varying in a range 4–7%, dependent on conditions (clear-sky or overcast) and wavelength range. Transmission by the foliage below 500 nm was found to be insignificant except for gaps that allowed unblocked view of the sky. The mean distribution of gaps derived from sky photographs explained observed differences between overcast and clear-sky conditions using diffuse sky radiance distributions from literature. Regarding reactive BVOC chemistry in the forest, the strong reduction of photolysis frequencies implied a major disruption of primary OH production and photochemical conversion. On the other hand, a large fraction of monoterpene loss within the forest was attributed to daytime NO_3 radicals that benefited from reduced photolysis and reduced NO concentrations. However, the resulting total in-forest degradations of 0.8% for isoprene and 3.4% for monoterpenes were considered insignificant.

[52] **Acknowledgments.** The author thanks R. Koppmann for organizing the ECHO project and campaigns, F. Rohrer and A. Hofzumahaus for useful discussions, and NIKON Germany (Düsseldorf) for providing a fish-eye objective. Financial support of the ECHO project by the German Bundesminister für Bildung und Forschung under grant 07 ATF 47 is gratefully acknowledged.

References

Ammann, C., C. Spirig, A. Neftel, M. Steinbacher, M. Komenda, and A. Schaub (2004), Application of PTR-MS for measurements of biogenic VOC in a deciduous forest, *Int. J. Mass Spectrum.*, *239*, 87–101.

Atkinson, R., and J. Arey (2003), Atmospheric degradation of volatile organic compounds, *Chem. Rev.*, *103*, 4605–4638.

Atkinson, R., D. L. Baulch, R. A. Cox, J. N. Crowley, R. F. Hampson, R. G. Hynes, M. E. Jenkin, M. J. Rossi, and J. Troe (2004), Evaluated kinetic and photochemical data for atmospheric chemistry: Part 1—Gas phase reactions of O_x, HO_x, NO_x and SO_x species, *Atmos. Chem. Phys.*, *4*, 1461–1738.

Aubrun, S., and B. Leitl (2004), Development of an improved physical modelling of a forest area in a wind tunnel, *Atmos. Environm.*, *38*, 2797–2801.

Aubrun, S., R. Koppmann, B. Leitl, M. Möllmann-Coers, and A. Schaub (2005), Physical modelling of a complex forest area in a wind tunnel—Comparison with field data, *Agric. For. Meteorol.*, *129*, 121–135.

Bohn, B., and H. Zilken (2005), Model-aided radiometric determination of photolysis frequencies in a sunlit atmosphere simulation chamber, *Atmos. Chem. Phys.*, *5*, 191–206.

Bohn, B., R. Koppmann, and F. Rohrer (2006), Seasonal variations and profile measurements of photolysis frequencies $j(O^1D)$ and $j(NO_2)$ at the ECHO forest field site, *J. Geophys. Res.*, *111*, D12303, doi:10.1029/2005JD006856.

Bongartz, A., J. Kames, U. Schurath, C. George, P. Mirabel, and J. L. Ponche (1994), Experimental determination of HONO mass accommodation coefficients using two different techniques, *J. Atmos. Chem.*, *18*, 149–169.

Chen, J. M., and J. Cihlar (1995), Plant canopy gap-size analysis theory for improving optical measurements of leaf area index, *Appl. Opt.*, *34*, 6211–6222.

Chen, J. M., P. M. Rich, S. T. Gower, J. M. Norman, and S. Plummer (1997), Leaf area index of boreal forests: Theory, techniques, and measurements, *J. Geophys. Res.*, *102*, 29,429–29,443.

Eller, B. M., R. Glättli, and B. Flach (1981), Optische Eigenschaften und Pigmente von Sonnen- und Schattenblättern der Rotbuche und der Blutbuche, *Flora*, *171*, 170–185.

Feister, U., and R. Grewe (1995), Spectral albedo measurements in the UV and visible region over different types of surfaces, *J. Photochem. Photobiol.*, *62*, 736–744.

Fuentes, J. D., et al. (2000), Biogenic hydrocarbons in the atmospheric boundary layer: A review, *Bull. Am. Meteorol. Soc.*, *81*, 1537–1575.

Grant, R. H., and G. M. Heisler (1997), Obscured overcast sky radiance distributions for ultraviolet and photosynthetically active radiation, *J. Appl. Meteorol.*, *36*, 1336–1345.

Grant, R. H., G. M. Heisler, and W. Gao (1997), Clear sky radiance distributions in ultraviolet wavelength bands, *Theoret. Appl. Climatol.*, *56*, 123–135.

Guenther, A., et al. (1995), A global model of volatile organic compound emissions, *J. Geophys. Res.*, *100*, 8873–8892.

Guenther, A., C. Geron, T. Pierce, B. Lamb, P. Harley, and R. Fall (2000), Natural emissions of non-methane volatile organic compounds, carbon monoxide, and oxides of nitrogen from North America, *Atmos. Environ.*, *34*, 2205–2230.

Heisler, G. M., R. H. Grant, and W. Gao (2003), Individual- and scattered-tree influences on ultraviolet irradiance, *Agric. For. Meteorol.*, *120*, 113–126.

Hofzumahaus, A., A. Kraus, and M. Müller (1999), Solar actinic flux spectroradiometry: A technique for measuring photolysis frequencies in the atmosphere, *Appl. Opt.*, *38*, 4443–4460.

Hofzumahaus, A., A. Kraus, A. Kylling, and C. S. Zerefos (2002), Solar actinic radiation (280–0420 nm) in the cloud-free troposphere between ground and 12 km altitude: Measurements and model results, *J. Geophys. Res.*, *107*(D18), 8139, doi:10.1029/2001JD900142.

Kleffmann, J., T. Gavriloaiei, A. Hofzumahaus, F. Holland, R. Koppmann, L. Rupp, E. Schlosser, M. Siese, and A. Wahner (2005), Daytime formation of nitrous acid: A major source of OH radicals in a forest, *Geophys. Res. Lett.*, *32*, L05818, doi:10.1029/2005GL022524.

Makar, P. A., J. D. Fuentes, D. Wang, R. M. Staebler, and H. A. Wiebe (1999), Chemical processing of biogenic hydrocarbons within and above a deciduous forest, *J. Geophys. Res.*, *104*, 3581–3603.

Malicet, J., D. Daumont, J. Charbonnier, C. Parisse, A. Chakir, and J. Brion (1995), Ozone UV spectroscopy II: Absorption cross-sections and temperature dependence, *J. Atmos. Chem.*, *21*, 263–273.

Matsumi, Y., F. J. Comes, G. Hancock, A. Hofzumahaus, A. J. Hynes, M. Kawasaki, and A. R. Ravishankara (2002), Quantum yields for production of $O(^1D)$ in the ultraviolet photolysis of ozone: Recommendation based on evaluation of laboratory data, *J. Geophys. Res.*, *107*(D3), 4024, doi:10.1029/2001JD000510.

Meller, R., and G. K. Moortgat (2000), Temperature dependence of the absorption cross sections of formaldehyde between 223 and 323 K in the wavelength range 225–375 nm, *J. Geophys. Res.*, *105*, 7089–7101.

Merienne, M. F., A. Jenouvrier, and B. Coquart (1995), The NO_2 absorption spectrum: 1. Absorption cross-sections at ambient temperature in the 300–500 nm region, *J. Atmos. Chem.*, *20*, 281–297.

Myneni, R. B. (1991), Modeling radiative transfer and photosynthesis in 3-dimensional vegetation canopies, *Agric. For. Meteorol.*, *55*, 323–344.

Sander, S. P., et al. (2003), Chemical kinetics and photochemical data for use in atmospheric studies, Evaluation Number 14, *JPL 02-25*.

Scurlock, J. M. O., G. P. Asner, and S. T. Gower (2001), Global Leaf area index data from field measurements, 1932–2000, data set, Oak Ridge Natl. Lab. Distrib. Active Arch. Cent., Oak Ridge, Tenn. (Available at http://www.daac.ornl.gov)

Shetter, R. E., et al. (2003), Photolysis frequency of NO_2: Measurement and modelling during the International Photolysis Frequency Measurement and Modelling Intercomparision (IPMMI), *J. Geophys. Res.*, *108*(D16), 8544, doi:10.1029/2002JD002932.

Spirig, C., et al. (2005), Eddy covariance flux measurements of biogenic VOCs during ECHO 2003 using proton transfer reaction mass spectrometry, *Atmos. Chem. Phys.*, *5*, 465–481.

Stroud, C., P. Makar, T. Karl, A. Guenther, C. Geron, A. Turnipseed, E. Nemitz, B. Baker, M. Potosnak, and J. D. Fuentes (2005), Role of canopy-scale photochemistry in modifying biogenic-atmosphere exchange of reactive terpene species: Results from the CELTIC field study, *J. Geophys. Res.*, *110*, D17303, doi:10.1029/2005JD005775.

Tanner, V., and B. M. Eller (1986), Veränderungen der spektralen Eigenschaften der Blätter der Buche von Laubaustrieb bis Laubfall, *Allgem. Forst Jagdzeitung*, *157*, 108–117.

Troe, J. (2000), Are primary quantum yields of NO_2 photolysis at $\lambda \leq$ 398 nm smaller than unity?, *Z. Phys. Chem.*, *214*, 573–581.

Webb, A. R., A. Kylling, M. Wendisch, and E. Jkel (2004), Airborne measurements of ground and cloud spectral albedos under low aerosol loads, *J. Geophys. Res.*, *109*, D20205, doi:10.1029/2004JD004768.

B. Bohn, Institut für Chemie und Dynamik der Geosphäre II: Troposphäre, Forschungszentrum Jülich, D-52425 Jülich, Germany. (b.bohn@fz-juelich.de)